1 **Electronic Supplementary Information**

2 ***Observing atomically precise nanocluster aggregates in solution by mass***

3 ***photometry***

4 Jayoti Roy,[a] Ila Marathe,[b] Vicki Wysocki,[b] Thalappil Pradeep[†a,c]

5 [a]DST Unit of Nanoscience (DST UNS) & Thematic Unit of Excellence (TUE), Department of

6 Chemistry, Indian Institute of Technology Madras, Chennai 600036, India.

7 [b]Department of Chemistry and Biochemistry and Native Mass Spectrometry Guided Structural

8 Biology Center, The Ohio State University, Columbus, Ohio 43210, United States.

9 [c]International Centre for Clean Water, 2nd Floor, B-Block, IIT Madras Research Park,

10 Kanagam Road, Taramani, Chennai 600113, India.

11

12 **Table of contents**

1

2

3

4

5

6

7

8

9

**SI1. Synthesis and characterization of of phosphine-protected alloy nanoclusters**

We have synthesized diphosphineobutane- and chlorine-co-protected Ag-Au alloy nanoclusters using a single-step co-reduction method. There are only very few reports on phosphine- and halide-protected nanoclusters using a single-step reaction. Here, $Ag_{11-x}Au_x$ was synthesized by co-reducing a mixture of silver and gold precursors in the presence of diphosphine ligands in methanol and dicholoromethane as co-solvents. About 0.112 mmol $AgNO_3$ and 0.006 mmol $HAuCl_4.3H_2O$ were dissolved in 5 mL of methanol by keeping the total metal ion concentration at 0.118 mmol. To the mixture of Ag and Au precursors, ~ 75 mg of 1,4-bis-(diphenylphosphine)butane (DPPB), dissolved in 9 mL of dichloromethane (DCM), was added with constant stirring. After 20 min of stirring, 35 mg of $NaBH_4$ in 1 mL of ice-cold water was added. The colorless mixture immediately turned brown. After ~ 6-8 h of vigorous stirring in dark, the color of the entire solution turned orange and was kept for aging at 4 $^\circ$C for 24 h. The solution was rotary evaporated and extracted in methanol. During extraction, 10 mL of methanol was introduced to the product and then the solution was centrifuged several times at 8000 rpm for 4-5 min to remove excess DPPB and phosphine complexes as a precipitate. After that, the entire methanol solution was vacuum-dried, and finally, the nanoclusters were cleaned with DCM. The dried alloy nanocluster was dissolved in methanol and used for further characterization.

The nanocluster was characterized using positive mode ESI MS measurements. The nanocluster was dissolved in methanol. Waters Synapt G2-Si high-definition mass spectrometer (HDMS) was used to record the ESI MS spectrum. During measurements, capillary voltage was set at 3 kV, and desolvation gas flow was maintained at 450 L h^{-1}. The source and desolvation temperature were maintained at 100 and 150 °C.

SI2. Prediction of the structure of the NC

We tried to predict the structure of NC and its ligand orientation theoretically using the Avogadro software package with the universal force field (UFF) method.[1] Furthermore, to optimize the geometry of Ag-Au alloy NCs, we employed a conjugate gradient optimization algorithm with a simple line search technique, and energy convergence of 10^{-6} eV.[2,3] Fig. 1(A) shows the optimized-NC structure. The Ag$_{11}$-

1 $_x$Au$_x$ core is surrounded by five P of monodentate DPPB ligands, while the remaining terminal P atoms

2 of the DPPB ligands are bound to five Cl atoms. This bonding configuration may be responsible for the

3 aggregation observed in response to changes in the solvent polarity. We also attempted to optimize the

4 NC structure by attaching all phosphorus atoms as bidentate ligands to the Ag$_{11-x}$Au$_x$ core. However,

5 this structural modification did not reach convergence and resulted in complete distortion of the

6 structure. Therefore, we considered that the initial structure, with monodentate P, was the most likely

7 one for this NC. The system shows solvent-dependent aggregation as reported previously.[4] To calculate

8 the specific volume of the vesicle-like nanoaggregates, we considered the NC to be spherical in nature.

9 Therefore, we used van der Waals diameter in our calculation (see Fig. S1).

10

11

12

13

14

15
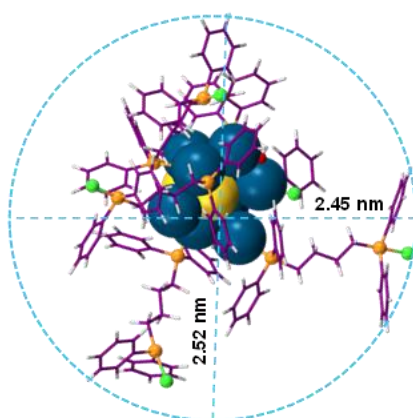
Fig. S1 The spherical structure of the NC with its van der Waals diameter (i.e., ~ 2.48 nm).

16

17 **SI3. Sample preparation for MP characterization**

18 Approximately 15 mg of nanocluster was formed during each set of the synthesis. MP is a label-free

19 single-particle analysis technique. For the MP measurements, 1.35 mg of nanocluster was dissolved

20 in 1 ml of methanol to prepare a working stock (~ 5 μM).

21 For the MP studies of solvent-induced aggregation with varying water % (i.e., $f_{water\%}$), 6 sets of

22 reactions were prepared. methanol and water at different ratios were added to each set by keeping the

23 final volume fixed to 100 μL. To each set, 10 μL of stock solution of nanocluster (~ 500 nM) was

24 added.

During each set of MP acquisition, unless otherwise stated 10 μL of solvent mixture was carefully placed in the sample gasket, and then after focusing the object well, 10 μL of 500 nM nanocluster solution was added and mixed well. The final concentration of nanocluster present in the silicone gasket wells was 50 nM (i.e., optimum concentration range for TwoMP).

SI4. Mass photometry measurements

Mass photometry is an analytical technique that is used to determine the mass of a sample by measuring the amount of light it scatters during particle landing events on the coverslip. It relies on the relationship between the mass of a particle and its optical properties. This method was already employed to distinguish 24-mer of Apoferritin proteins from Fe^{3+} metal ions containing holoferritin nanocages.[5] Utilizing MP in such systems opens up new directions to implement this technique in nanomaterials. Instrumental methods used for mass photometric experiments are described below.

1)   **Measurement, solution preparation, and instrument operation**. For the MP measurements, 15 μL of a specific solvent mixture, i.e., 70% water and 30% of methanol, was used to find focus by the objective lens through the 'Droplet-Dilution Find Focus' method in AcquireMP (Refeyn) software. This particular solvent mixture was prepared in such a way that the calibrants, as well as the nanocluster aggregates, are stable during the acquisition. After focusing the droplet on top of the glass slide, 5 μL of the NC solutions prepared at different solvent mixture was added to acquire particle landing events on the glass slide. The total solution volume during each measurement was fixed at (15 + 5) μL = 20 μL. The data was recorded as a movie by using the same software. Refeyn Two^{MP} mass photometer was used for the study.

2)   **Preparation of glass coverslips.** Glass coverslips (24 × 50 mm, Thorlabs) were cleaned thoroughly by rinsing alternatively with Milli-Q water and isopropanol for a minimum of 8 times, and then dried using a nitrogen stream and stored in a dry clean place until use. Silicone gaskets (6 cm ×

1   1 cm) were rinsed sequentially with Milli-Q water, isopropanol, and Milli-Q water, dried under a

2   nitrogen stream, and placed on the freshly cleaned coverslips.

3   3)   **Mass photometry setup.** All MP measurements were acquired on a Refeyn two[MP] mass

4   photometer with a 10.8×2.9 μm^2 field of view.

5   4)   **Calibration process.** 1:1 protein mixture, i.e., β-amylase (BA) (10 nM), and thyroglobulin

6   (TGA) (10 nM) were used as calibration mixture in 70% water:30% methanol. These proteins were

7   selected such that the protein mixture can be used to calibrate the mass range of interest (i.e., 50 – 660

8   kDa). Final concentration of each calibrant was 10 nM. We used the same acquisition method for each

9   sample analysis.

10

11   **SI5. Data processing**

12   Dynamic mass photometry movies were processed by treating each frame with a sliding medium

13   background subtraction algorithm with high spatiotemporal resolution using DiscoverMP software. In

14   brief, each frame was divided by its local median, that is, the median of a pre-defined frame interval

15   (here 890 frames) centered around the frame of interest, to calculate the background-subtracted frames,

16   F:

17
$$Fi = \frac{X_i}{X_{i-100:i+100}}$$

18   Where X_i is the current raw frame and $X_{i-100:i+100}$ represents the median pixel values of raw frames, from

19   i-100 up to (and including) i+100.[6] Each background-subtracted frame was then additionally treated

20   with a two-dimensional (2D)-median noise filter to remove any large dynamic background sources (for

21   example, fluctuations in illumination, if present). The window size of 890 frames for the sliding median

22   algorithm was chosen during the acquisition of single particle landing events because it was the window

23   size that did not detrimentally affect particle contrast or contrast precision.

24   **SI6. Calculation of single particle mass during particle-landing events on the coverslip**

To measure accurate mass for the individual mass of the nanoaggregate of each set of measurements, we selected a particular spherical point spread function (PSF) from a particular ratiometric frame from the entire frames of a measurement. Then we inverted the selection spatially and temporally from the entire acquisition movie. This method enables us to measure the ratiometric contrast, as well as mass/es (in kDa) of individual particle/s accurately per count.[7–9]

We then calculated the kernel density estimate (KDE) plot from the area of each Gaussian distribution. The KDE is calculated as, $a = A\sigma\sqrt{(2\pi)}$, where a is the area, A is the amplitude and σ is the standard deviation of the fitted Gaussian.

Here, the equal binding rate of each nanoaggregates with the coverslip was considered as only Ag-Au alloy nanocluster, i.e., $[Ag_{11-x}Au_x(DPPB)_6Cl_2O_2]^{2+}$ [x = 0-5] was taken as the precursor for the entire study.

SI7. Calculation of the average mass of alloy-NCs

The composition of Au-doped nanocluster used here is $[Ag_{11-x}Au_x(DPPB)_5Cl_5O_2]^{2+}$ [X = 0-5], where DPPB represents 1,4-bis(diphenylphosphino)butane. In the mass spectrometric study, the Au-undoped and doped nanocluster ionizes at m/z 1808, 1852, 1897, 1942, and 1986 with varying ion intensities. To calculate the approximate number of nanoclusters that are present in the nanoaggregates, the following method is employed –

$$\frac{The\ central\ mass\ of\ nanoaggregates\ (observed\ in\ MS)}{The\ average\ mass\ of\ nanocluster\ (observed\ in\ MS)}$$

The intensity ratio (IR) of five nanoclusters (X = 0-5) = 4119.5:2932.3:2139.2:1583.3:1000.6

$$= 4:3:2:1.6:1$$

Total of IR = 11.6

The average mass/charge (m/z) of these Au-undoped and Au-doped nanoclusters =

$$\frac{\Sigma i \left(\frac{m}{z} \times z \times \frac{IR_i}{11.6}\right), i = 0-5}{z}$$

$$= \frac{3670.33}{2}$$

$$= 1835.16$$

SI8. Sample preparation for RT-TEM measurements

During RT-TEM measurements, 3 µL of NC-solution of binary solvent mixture was dropcasted directly on a regular carbon-coated Cu-grid and kept for drying (~ 10 min) before inserting the grid for the TEM-imaging.

SI9. Cryo-electron microscopy of nanoaggregates

Cryo-electron microscopy (cryo-EM) was performed using a Thermo Glacios cryo-EM instrument. To prepare the cryo-EM specimens, a 3 µL droplet of NC-solution was applied to a lacey carbon-coated copper TEM grid. The grid was then rapidly frozen in liquid ethane using the Vitrobot Mark from FEI in Eindhoven, The Netherlands. The freezing conditions involved maintaining a temperature of 4°C with 67% humidity. After vitrification, the grids were either directly transferred to the cryotransfer holder of the microscope or stored in liquid nitrogen until the EM measurements. The imaging took place at a temperature around 90 K. The TEM was operated at an acceleration voltage of 200 kV, and a defocus of the objective lens between 0.5 – 1 µm was applied to enhance contrast. Cryo-EM micrographs were recorded at various magnifications using a bottom-mounted 4k CMOS camera. The total electron dose in each micrograph was kept below 17 e$^-$/Å^2.

| Set	Water (%)	MeOH (%)	Mass (kDa)	No of NCs (Mw = ~3670)
1	40	60	47	13
2	50	50	65	18
3	60	60	83	23
4	70	30	93	26
5	80	20	103	29
6	90	10	84-183	23 - 50

Table S1 Calculation of the aggregation number (N_{NCs}) present per nanoaggregate as different solvent mixture.
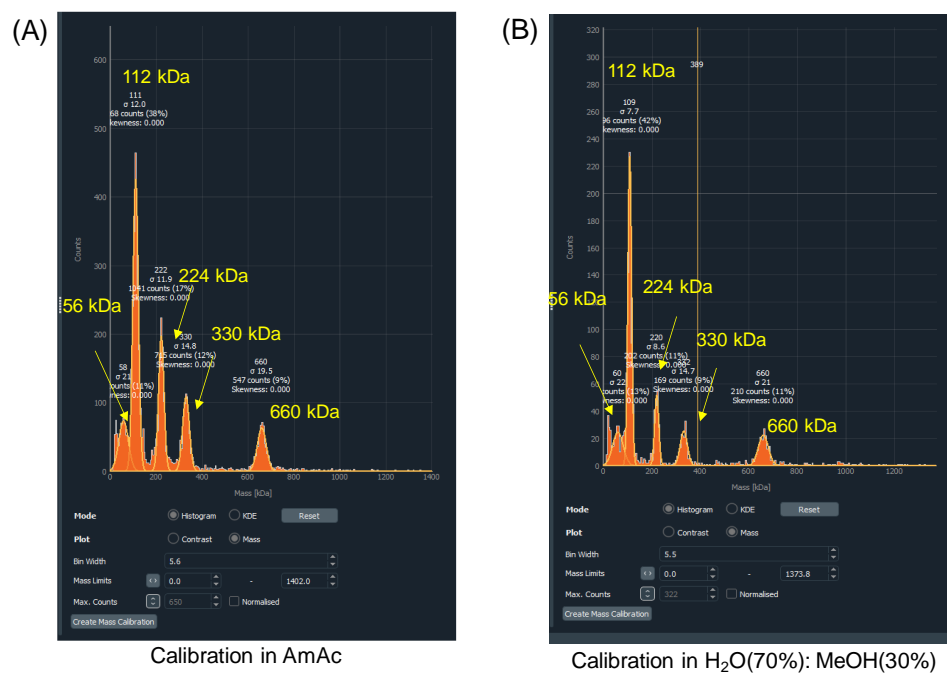
Fig. S2 Histogram of protein calibrants measured in (A) 100 μM ammonium acetate (AmAc) solution and (B) 70% water and 30% methanol mixture, by MP. Histograms collected from AcquireMP software. The masses of different oligomers are labelled in the histograms.
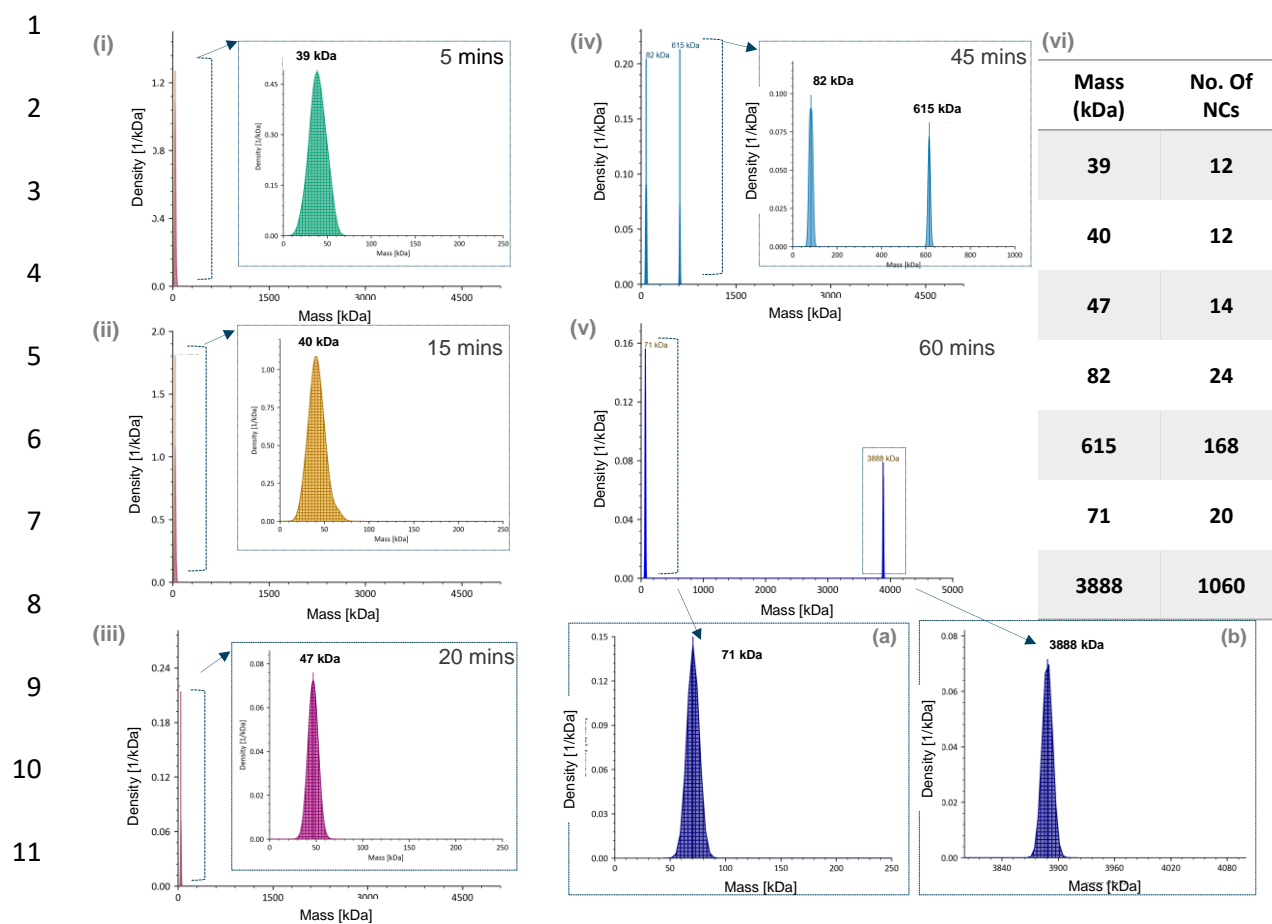
Fig. S3 Spatiotemporal selections of single particle landing event enables determining mass of single nanoaggregate for a particular measurement. **(A)(i-v)** Time-dependent MP histograms of size-evolution of single particle landing event of nanoaggregtaes at $f_{40\%}$ in the mass range of 0-5500 kDa. Inset of each histogram shows the expanded mass range labelled with average mass. (vi) Table shows the average number of parent nanocluster present per nanoaggregate.
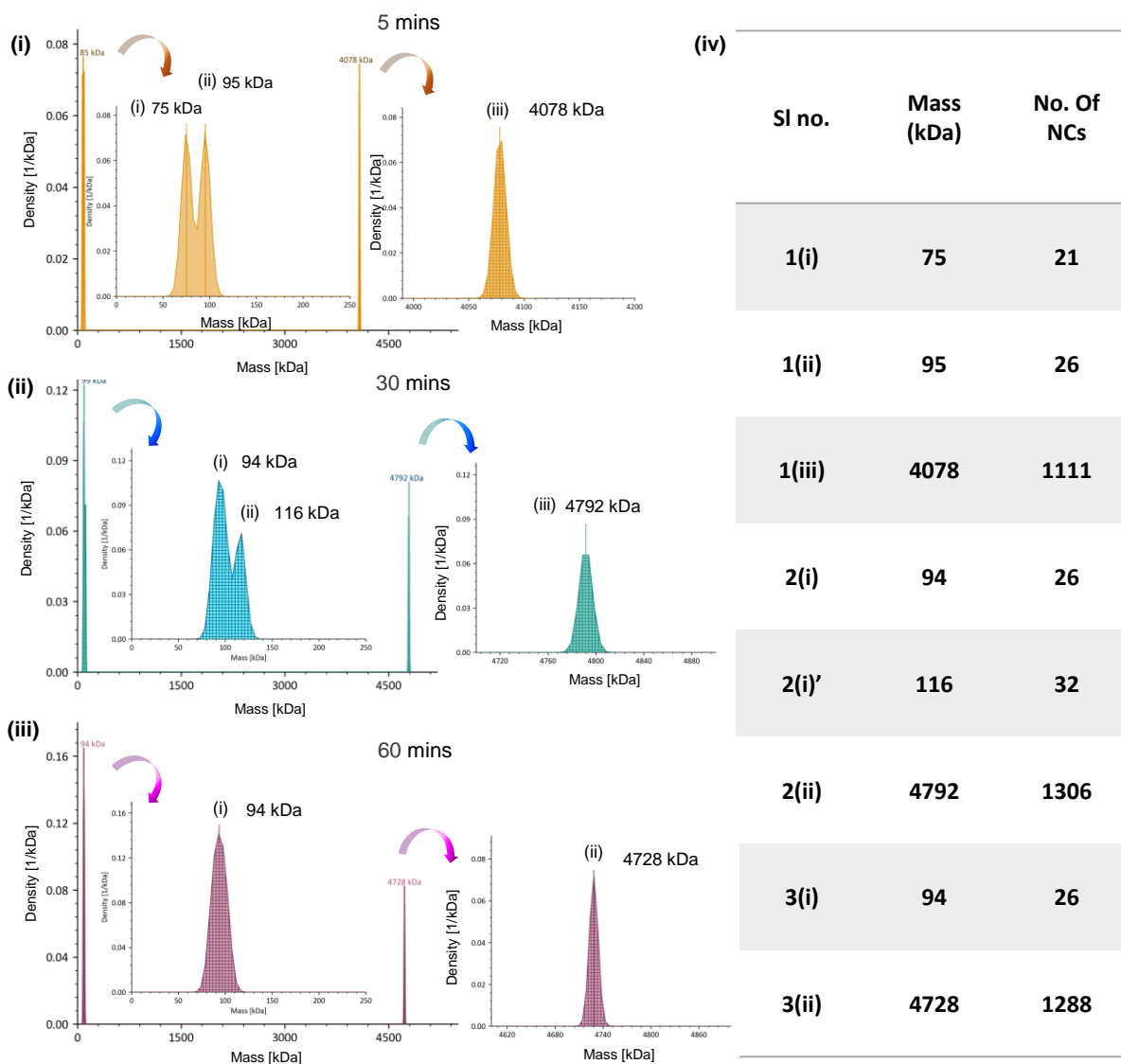
Fig. S4 Spatiotemporal selections of single particle landing event enables determining mass of single nanoaggregate for a particular measurement. **(A)** Time-dependent MP histograms of size-evolution of single particle landing event of nanoaggregtaes at $f_{80\%}$ in the mass range of 0-5500 kDa. Inset of each histogram shows the expanded mass range labelled with average mass. (vi) Table shows the average number of parent nanocluster present per nanoaggregate.
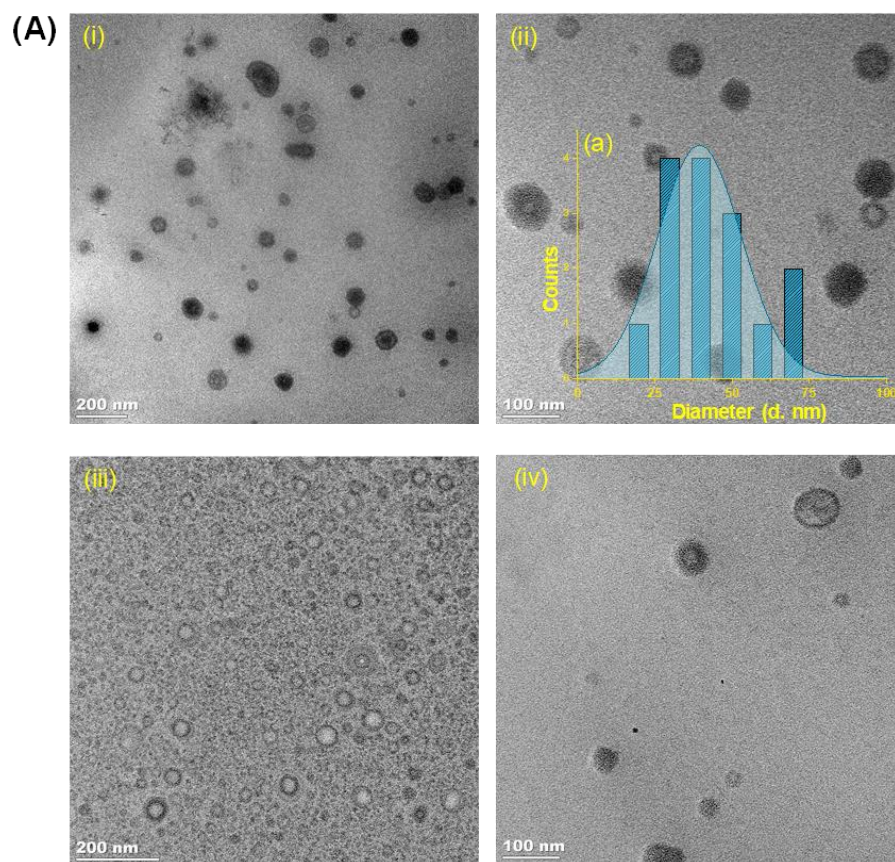
1

2
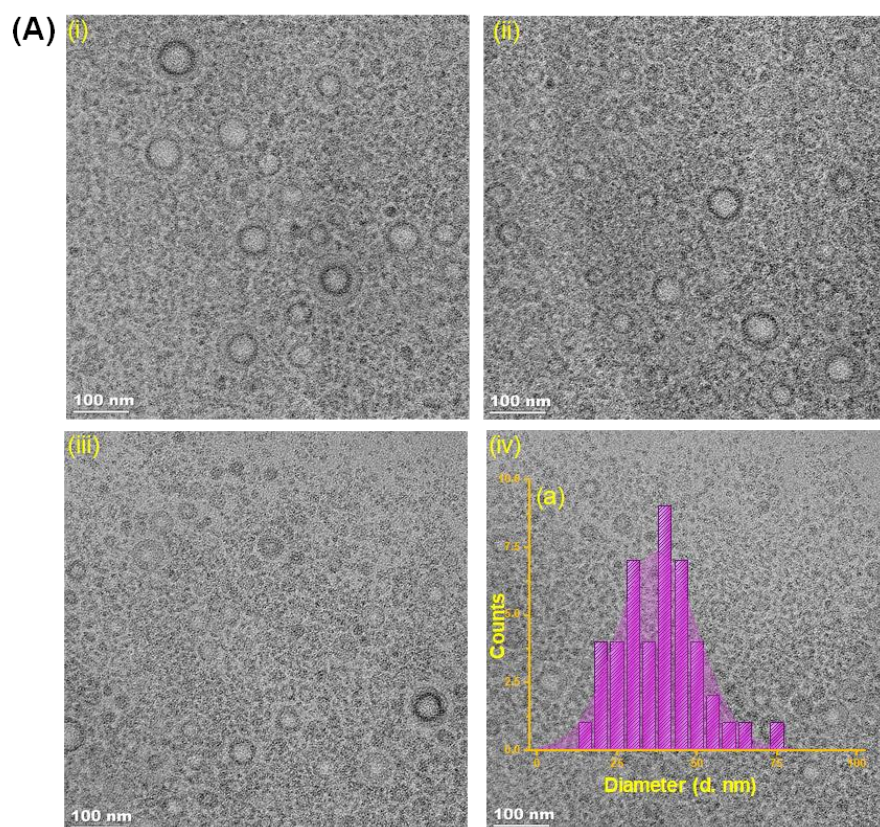
Fig. S5 (A) (i-iv) RT-TEM micrographs of alloy nanocluster-based nanoaggregates of $f_{40\%}$ at 0 min. Inset (a) shows the average particle size distributions observed at 0 min.
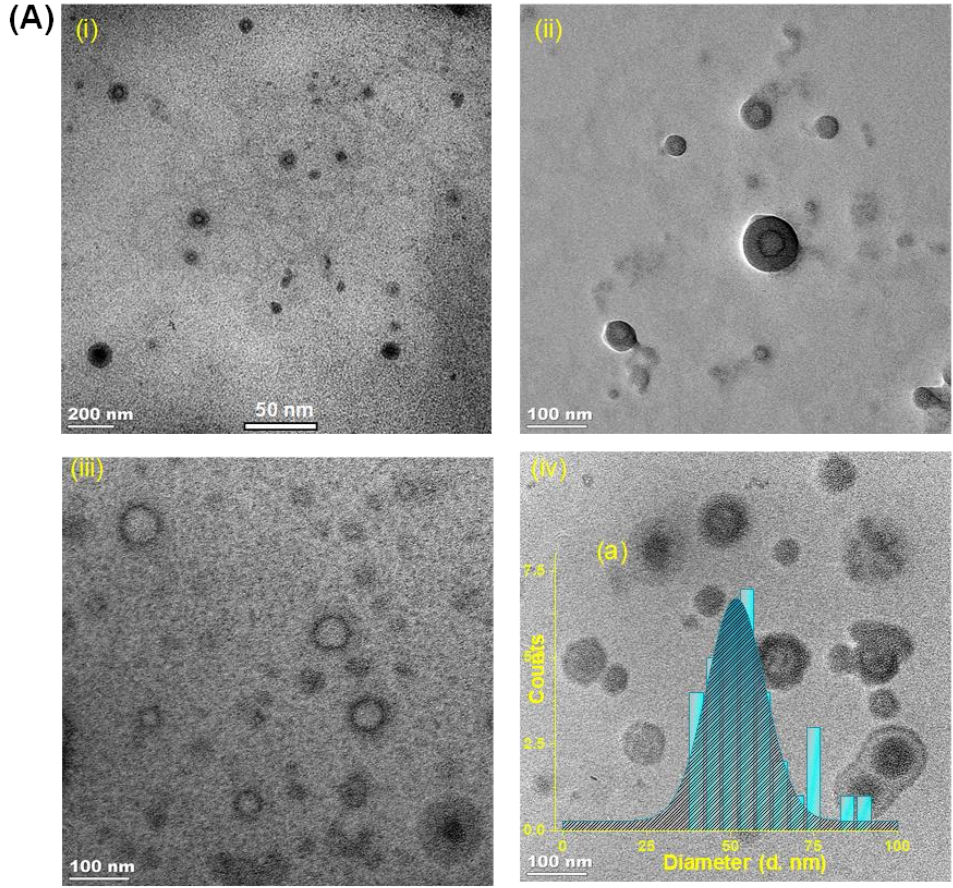
1

2

Fig. S6 (i-iv) RT-TEM micrographs of alloy nanocluster-based nanoaggregates of $f_{40\%}$ at 30 mins. (a) Inset shows average size-distribution of the nanoaggregates as a function of counts after 30 min.
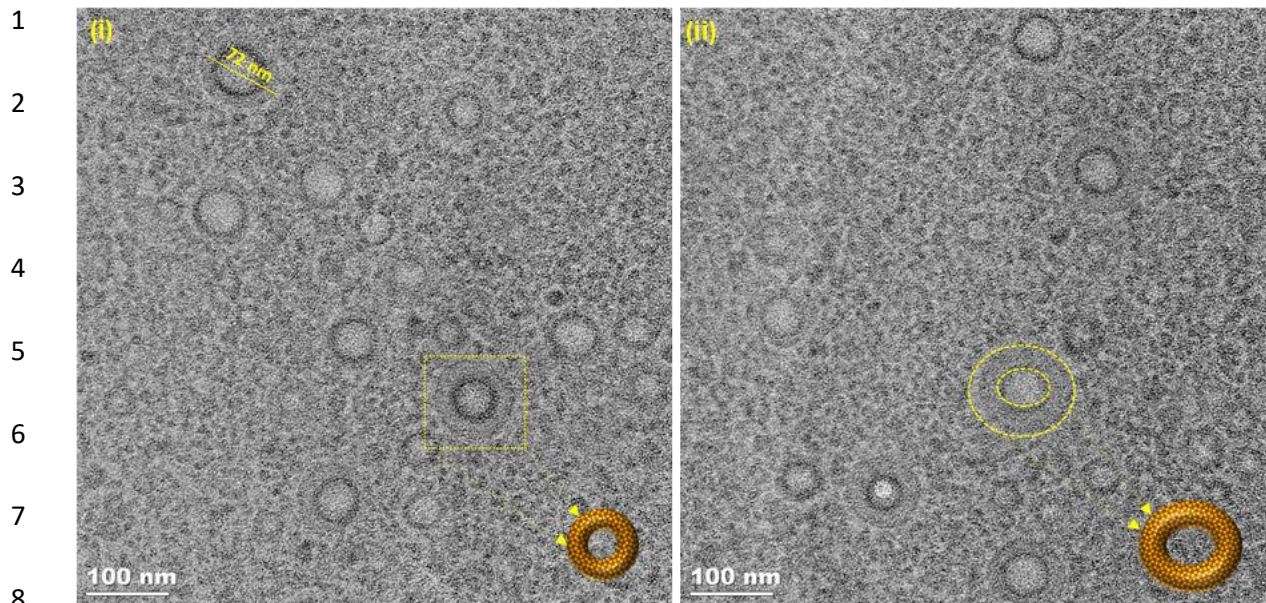
1

2

3

4

5

6

7

8

9

10

11

12

13

14 **Fig. S7 (A) (i-iv)** RT-TEM micrographs of alloy nanocluster-based nanoaggregates of $f_{40\%}$ at 60 min and inset (a) represents the particle-size distribution.

15

16

17

18

19

20

21

22

23
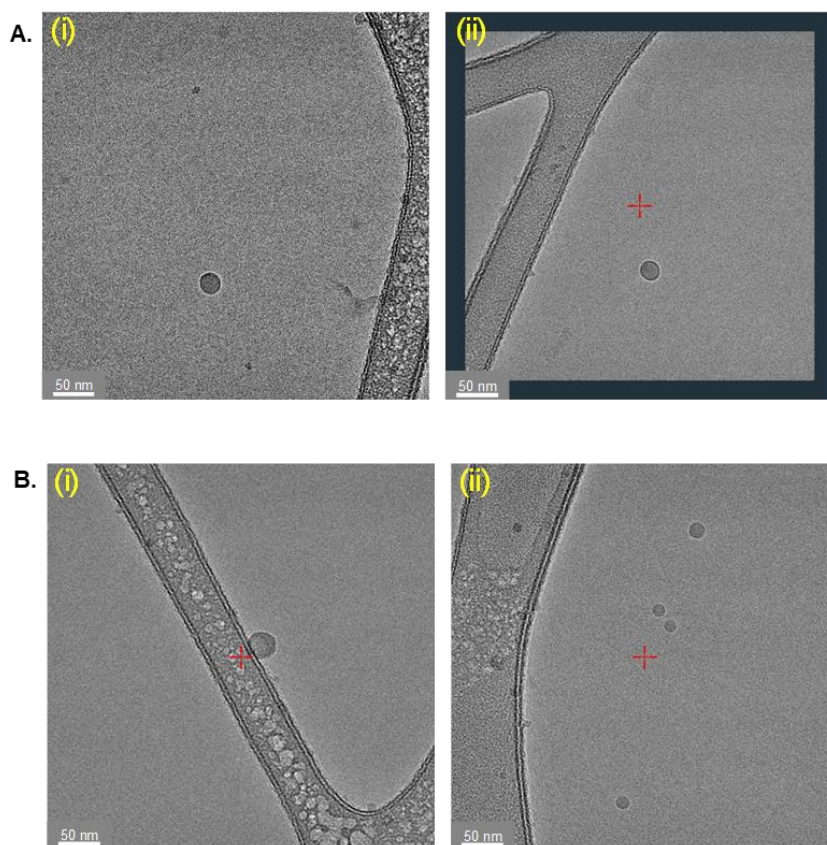
Fig. S8 Cryo-TEM micrographs of $f_{80\%}$ at (A) 0 min, and (B) 30 mins.
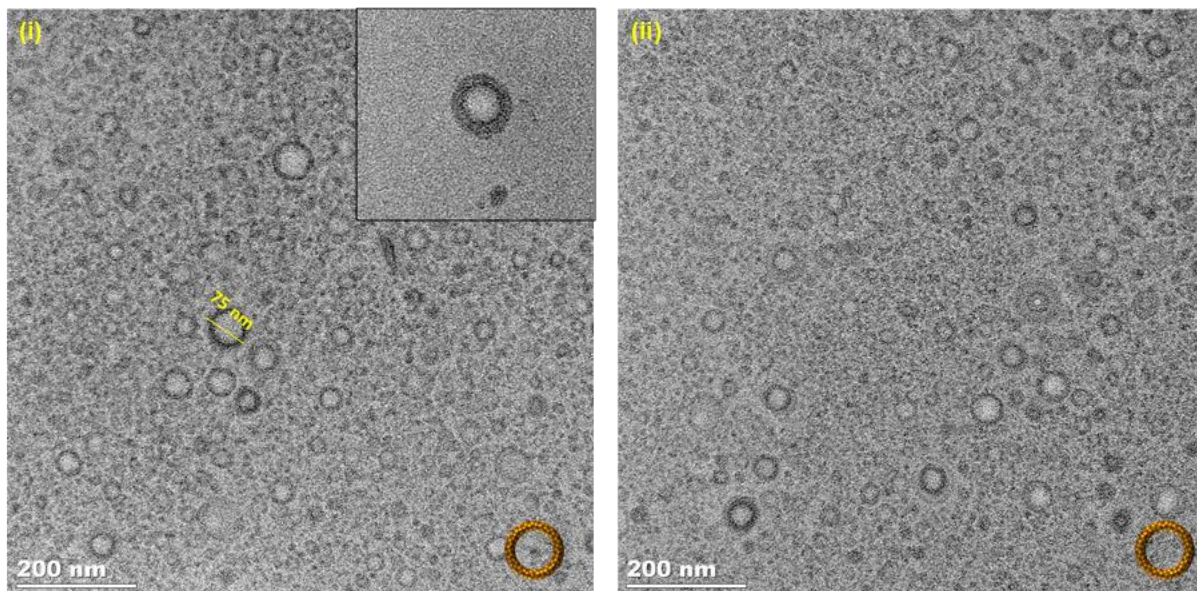
1

2

3

4

5

6

7

8

9

10

11

Fig. S9 RT-TEM micrographs of alloy nanocluster-based nanoaggregates of $f_{80\%}$ at 0 mins. Inset shows a schematic representation of the donut-shaped nanoaggregates.

Fig. S10 RT-TEM micrographs of alloy nanocluster-based nanoaggregates of $f_{80\%}$ at 30 mins. Inset shows a schematic representation of the donut-shaped nanoaggregates.

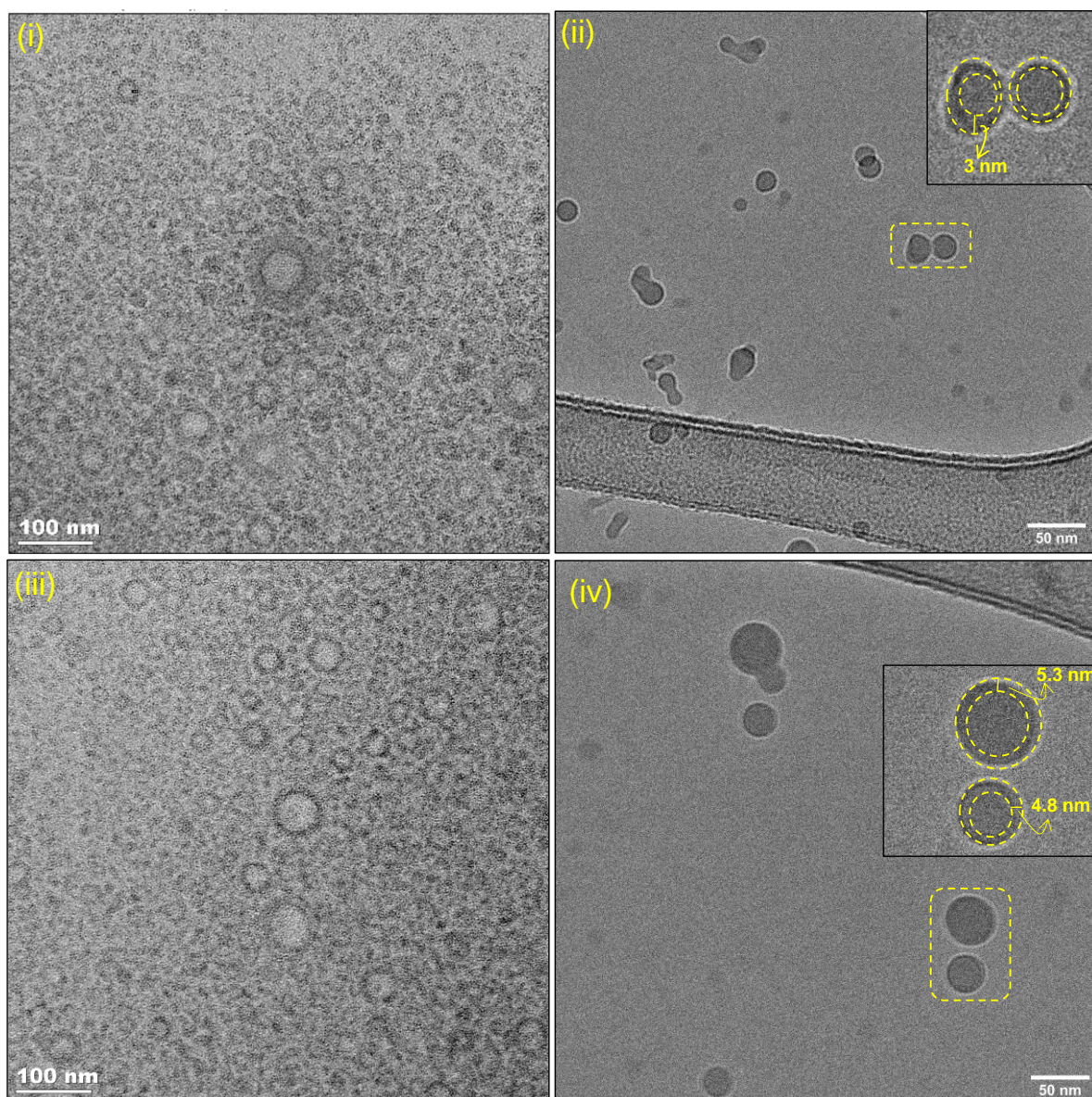**Fig. S11** RT-TEM and cryo-TEM micrographs of nanoaggregates forming at 0 min (i-ii) and at 30 min (iii-iv) of $f_{40\%}$, respectively. Insets of (ii) and (iv) show the expanded view of the vesicle-like structure of nanoaggregate with NC-shell (in nm).

1

2

3

4

5

6

Set	MP				Cryo-TEM				RT-TEM
$f_{water\%}$	Evolution time (min)	Mass (kDa)	Gaussian (σ)	N_{NC}s (Mw of NC = ~3670)	Evolution time (min)	Diameter range (nm)	Avg. radius (nm)	N_{NC}s/nano aggregate	Avg. thickness of the shell (nm)
$f_{40\%}$	0	39	14.4	~11	0	12.5 ± 5	6.25	~12	10.9
$f_{40\%}$	30	70	27.56	~19	30	33 ± 5	16.5	~21	15
$f_{40\%}$	60	86	28.49	~25	60	45 ± 15	22.5	-	16

Table S2 Comparison of masses (M_{av}s), gaussian (σ), radius, N_{NC}s of nanoaggregates, and thickness of the shell of the nanoaggregate determined at different times of evolution for $f_{40\%}$, from MP, cryo-TEM, and RT-TEM.

1

2 **SI11. Possible mechanism of formation and evolution of nanoaggregates**

3 The possible mechanism of formation of such hollow spherical superstructures was discussed in the

4 previous report.[13] The NC is completely soluble in methanol and consists of hydrophilic (Cl) and

5 hydrophobic (DPPB) counterparts in its ligand shell. To understand the details of solution phase self-

6 assembly of NCs encapsulated by DPPB and Cl ligands, we performed a series of time-dependent MP

7 measurements at $f_{40\%}$ and $f_{80\%}$. The self-assembly of NCs and the growth of nanoaggregates with

8 increasing dielectric constant are mainly attributed to π---π and C-H---π interactions between DPPB

9 ligands of alloy NCs, as discussed in previous research.[14] Over time, these aggregated assemblies of

10 NCs tend to reach a state of minimum surface energy, resulting in the formation of hollow vesicle-like

11 structures. Each individual vesicle continues to grow within the solution, with the rate of growth being

12 influenced by the polarity of the solvent and the availability of NC monomers in the solution. This

13 growth process continues until the vesicles reach a threshold diameter, beyond which no further growth

is discernible. Three major phenomena were observed in terms of mass calculation of such nanoaggregates in solution. First, with increase in water percentage (see Fig. 1C), a greater number of NCs assembled to form nanoaggregates with increased molecular mass. This is in accordance with a previous report where with increase in water, thick-walled nanoaggregates were formed.[13] Second, at $f_{90\%}$, the overall Mav decreased compared to that at $f_{80\%}$. We attribute such phenomena to rapid agglomeration due to a sudden increase in the solvent polarity which effectively reduced the size of the nanoaggregates to retain the spherical morphology. Moreover, it is already known that higher amount of water in a water-methanol binary solvent system causes fast aggregation.[15] Lastly, at a constant water-methanol ratio (i.e., at $f_{40\%}$), initially smaller aggregates were noticed, presumably due to high solubility of NCs in methanol. However, these smaller aggregates grew with time. This is more-likely due to enthalpy driven self-assembly, associated with hydrophobicity of the DPPB ligands (see Fig. 2A and Fig. 3).[14] The growth of nanoaggregates was observed systematically e.g., at $f_{50\%}$, $f_{60\%}$, and $f_{70\%}$.

SI12. Correlation between MP and cryo-TEM measurements

We carried out a side-by-side comparison of the MP and cryo-TEM workflows along with the size evolution of nanoaggregates. At $f_{40\%}$, the MP study showed that the average NC, at 1 min of the measurements is ~12 (see table in Fig. SI2). In corollary, cryo-TEM measurements at 5 min showed an average particle size-distribution of 12.5 ± 5 nm. The average van der Waals diameter of individual NC was ~2.48 nm (measured from computationally optimized NC). To calculate the specific volume of the vesicle-like nanoaggregates, we considered the NC to be spherical in nature. Therefore, we used van der Waals diameter in our calculation. Combining RT-TEM and cryo-TEM studies, we confirmed that NCs are aggregating in solution as hollow spheres, as suggested previously.[4] The density of a nanoaggregate can be estimated by dividing the average mass, as determined by MP, by its average volume, which is derived from cryo-TEM measurements. For instance, at $f_{40\%}$ and after 60 min, the nanoaggregates exhibit an average mass of 86 kDa and a diameter of 45 nm. This results in a calculated density of ~ 0.003 g/cm³. This density is considerably lower than that of bulk water and methanol, which have densities of 1 and 0.792 g/cm³, respectively. The deviation could be arising from an under-estimation of the mass by MP or over-estimation of the size by cryo-TEM. Therefore, correlating the findings with more established single molecule mass determination techniques like charge detection mass spectrometry (CDMS) could enhance the

measurement accuracy, an area that requires further investigation in future. Such a correlation with CDMS has additional issues as gas phase ions produced by electrospray ionization may lose some or all the solvent molecules or the aggregate ions may be fragmented.

References

1 A. K. Rappe, C. J. Casewit, K. S. Colwell, W. A. Goddard III and W. M. Skiff, *Journal of the American Chemical Society*, 2002, **114**, 10024–10035.

2 J. Hafner, *Journal of Computational Chemistry*, 2008, **29**, 2044–2078.

3 J. P. Perdew, J. A. Chevary, S. H. Vosko, K. A. Jackson, M. R. Pederson, D. J. Singh and C. Fiolhais, *Physical Review B*, 1992, **46**, 6671.

4 M. Jash, A. Jana, A. K. Poonia, E. Khatun, P. Chakraborty, A. Nagar, T. Ahuja, K. V. Adarsh and T. Pradeep, *Chemistry of Materials*, 2023, **35**, 313–326.

5 TwoMP Mass Photometer for Protein Characterization | Refeyn, https://www.refeyn.com/twomp-mass-photometer, (accessed 18 July 2023).

6 A. Sonn-Segev, K. Belacic, T. Bodrug, G. Young, R. T. VanderLinden, B. A. Schulman, J. Schimpf, T. Friedrich, P. V. Dip, T. U. Schwartz, B. Bauer, J.-M. Peters, W. B. Struwe, J. L. P. Benesch, N. G. Brown, D. Haselbach and P. Kukura, *Nature Communications*, 2020, **11**, 1772.

7 S. H. Lai, S. Tamara and A. J. R. Heck, *iScience*, 2021, **24**, 103211.

8 D. Wu, P. Hwang, T. Li and G. Piszczek, *Gene Therapy 2021 29:12*, 2022, **29**, 691–697.

9 D. Wu and G. Piszczek, *European Biophysics Journal*, 2021, **50**, 403–409.

10 H. Fischer, I. Polikarpov and A. F. Craievich, *Protein Science*, 2004, **13**, 2825–2828.

11 C. Takai, H. Watanabe, T. Asai and M. Fuji, *Colloids and Surfaces A: Physicochemical and Engineering Aspects*, 2012, **404**, 101–105.

12 N. J. Warren, O. O. Mykhaylyk, A. J. Ryan, M. Williams, T. Doussineau, P. Dugourd, R. Antoine, G. Portale and S. P. Armes, *Journal of the American Chemical Society*, 2015, **137**, 1929–1937.

13 M. Jash, A. Jana, A. K. Poonia, E. Khatun, P. Chakraborty, A. Nagar, T. Ahuja, K. V Adarsh and T.

1   Pradeep, *Chemistry of Materials*, 2023, **35**, 313–326.

2   14   A. Singh, G. R. Nair, P. Liplap, Y. Gariepy, V. Orsat and V. Raghavan, *Antioxidants*, 2014, **3**, 99–113.

3   15   M. P. Kelley, P. Yang, S. B. Clark and A. E. Clark, *Inorganic Chemistry*, 2018, **57**, 10050–10058.

4